ACS Catalysis

Research Article

pubs.acs.org/acscatalysis

Selective Catalytic Hydrogenolysis of Carbon−Carbon σ Bonds in Primary Aliphatic Alcohols over Supported Metals

Lu Di,[†,∥] Sikai Yao,[†,∥] Mengru Li,[‡] Guangjun Wu,[†] Weili Dai,[†] Guichang Wang,[‡] Landong Li,*[,†,§] and Naijia Guan[†,§]

[†]School of Materials Science and Engineering & National Institute for Advanced Materials, [‡]Center of Theory and Computational Chemistry, College of Chemistry, and [§]Key Laboratory of Advanced Energy Materials Chemistry of the Ministry of Education, Collaborative Innovation Center of Chemical Science and Engineering, Nankai University, Tianjin 300071, People's Republic of China

Supporting Information

ABSTRACT: The selective scission of chemical bonds is always of great significance in organic chemistry. The cleavage of strong carbon−carbon σ bonds in the unstrained systems remains challenging. Here, we report the selective hydrogenolysis of carbon−carbon σ bonds in primary aliphatic alcohols catalyzed by supported metals under relatively mild conditions. In the case of 1-hexadecanol hydrogenolysis over Ru/TiO_2 as a model reaction system, the selective scission of carbon−carbon bonds over carbon−oxygen bonds is observed, resulting in *n*-pentadecane as the dominant product with a small quantity of *n*-hexadecane. Theoretical calculations reveal that the 1-hexadecanol hydrogenolysis on flat Ru (0001) undergoes two parallel pathways: i.e. carbon−carbon bond scission to produce *n*-pentadecane and carbon−oxygen bond scission to produce *n*-hexadecane. The removal of adsorbed CO on a flat Ru (0001) surface is a crucial step for the 1-hexadecanol hydrogenolysis. It contributes to the largest energy barrier in *n*-pentadecane production and also retards the rate for *n*-hexadecane production by covering the active Ru (0001) surface. The knowledge presented in this work has significance not just for a fundamental understanding of strong carbon−carbon σ bond scission but also for practical biomass conversion to fuels and chemical feedstocks.

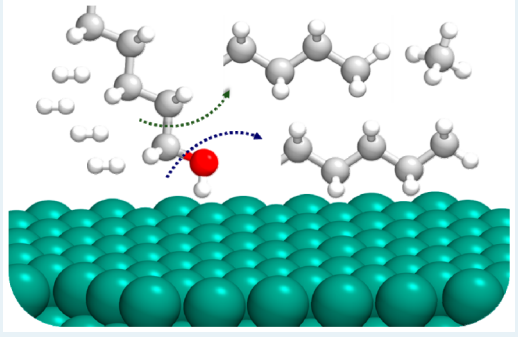

KEYWORDS: *ruthenium catalyst, primary aliphatic alcohols, hydrogenolysis, carbon−carbon bond scission, theoretical calculations*

INTRODUCTION

Carbon−carbon single bonds, i.e. σ bonds, are the most abundant in natural organic compounds, and their cleavage is of great significance in organic transformations. However, the cleavage of carbon−carbon σ bonds is challenging because of the strength and stability of these linkages, especially in the unstrained systems. Therefore, tactfully designed catalyst systems, delicately selected substrates, and their compatibility are strictly required to realize this process. For example, a metal−organic cooperative protocol has been successfully applied in the cleavage of carbon−carbon σ bonds with adjacent carbonyl groups under special driving force from a chelation auxiliary.[1,2] Another known example is dioxygenase-type carbon−carbon bond cleavage with metalloenzymes, as in natural biological systems.[3−5] Hydrogenolysis has been acknowledged as a very simple but efficient strategy for the cleavage of strong chemical bonds: e.g., carbon−oxygen bonds.[6,7] The hydrogenolysis of unstrained carbon−carbon σ bonds in benzyl Meldrum acids has been achieved by using homogeneous Pd catalyst under mild conditions.[8] More recently, the hydrogenolysis of carbon−carbon bonds in secondary benzyl alcohol was reported with homogeneous Rh catalysts directed by N-containing groups.[9] In fact, early studies indicated that the heterogeneous Ni/Al_2O_3 system could catalyze the hydrogenolysis of carbon−carbon bonds for the dealkylation of cage hydrocarbons, i.e. polyalkyladamantanes, at high temperatures.[10,11] The successive hydrogenolysis of various saturated hydrocarbons has been extensively investigated with Ni/Al_2O_3,[12,13] Pt/Al_2O_3[14,15] and silica-supported metal hydrides[16−19] as heterogeneous catalysts. For the cleavage of carbon−carbon bonds via hydrogenolysis, a very interesting old study demonstrated that the hydrogenolysis of primary alcohols to hydrocarbons with one less carbon could be achieved over a nickel catalyst under harsh conditions: i.e., at 10−20 MPa of H_2 and 523 K.[20]

Herein we present the first systematic investigation on the hydrogenolysis of carbon−carbon bonds in primary aliphatic alcohols, known as typical platform chemicals derived from triglycerides and other biomass resources, catalyzed by various supported metals under relatively mild conditions. We will focus on catalyst-controlled selective bond fission and the mechanistic aspects of such reactions via theoretical calcu-

Received: July 23, 2015
Revised: October 24, 2015
Published: October 28, 2015

DOI: 10.1021/acscatal.5b02180
ACS Catal. 2015, 5, 7199−7207

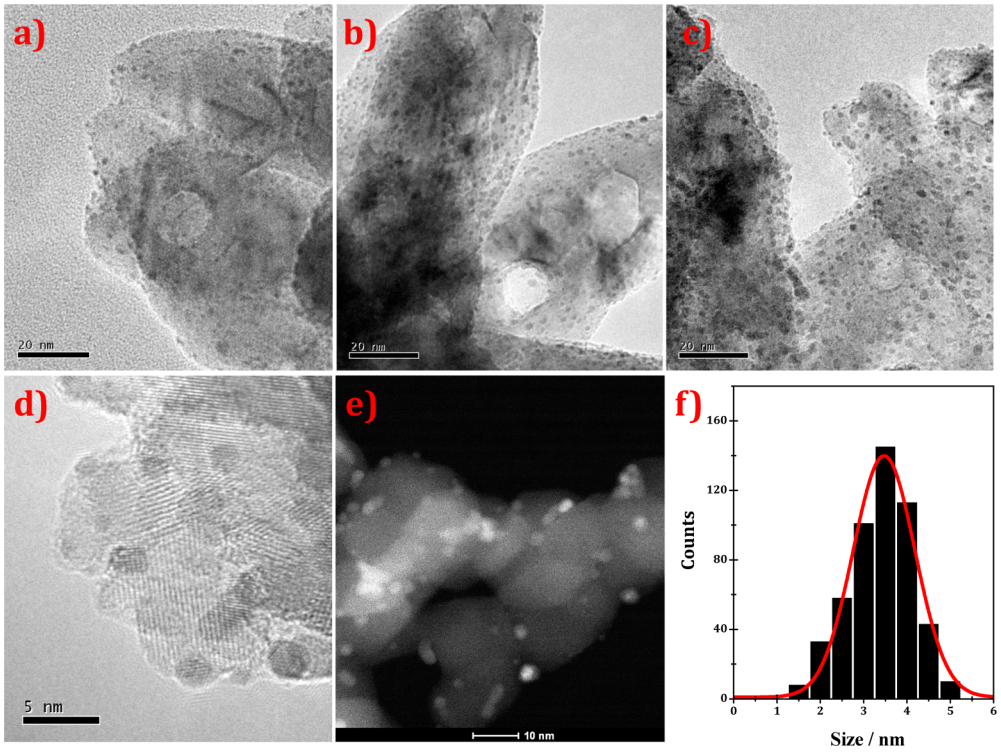

Figure 1. (a–c) TEM images of (a) 0.96% Ru/TiO_2, (b) 1.62% Ru/TiO_2, and (c) 3.18% Ru/TiO_2, (d) high-resolution TEM and (e) high-angle annular dark field scanning TEM images of 1.62% Ru/TiO_2, and (f) Ru particle size distribution in 1.62% Ru/TiO_2.

lations. The obtained knowledge is not only of fundamental significance for an understanding of the reactivity and cleavage of strong carbon–carbon σ bonds but also of practical significance for biomass conversion to fuels and chemical feedstocks via hydrodeoxygenation.[21−25] The rational design of catalysts and reaction systems guided by reaction mechanisms makes it possible to develop a synthetic strategy for targeted heterogeneous organic transformations.

EXPERIMENTAL SECTION

Preparation of Supported Metal Catalysts. Commercially available oxides, i.e. SiO_2 (Sinopec, surface area 206.2 m^2/g), ZrO_2 (Alfa, surface area 69.5 m^2/g), TiO_2 (Alfa, surface area 67.3 m^2/g), and CeO_2 (Acros, surface area 50.6 m^2/g), were calcined in flowing air at 673 K for 6 h and then used as catalyst supports. Diffluent metal salts ($H_2PtCl_6{\cdot}xH_2O$, $PdCl_2$, $RuCl_3{\cdot}xH_2O$, $RhCl_3{\cdot}xH_2O$ and $H_2IrCl_6{\cdot}6H_2O$, all from Acros) were dissolved in distilled water to derive aqueous solutions with a metal concentration of 1.0 mg/mL and then used as precursors for supported metals. The catalysts were prepared by impregnating the supports with aqueous solutions of metal salts in a rotary evaporator at constant temperature. In a typical preparation process of Ru/TiO_2, 18 mL of $RuCl_3$ aqueous solution was added to 1 g of TiO_2 support. The impregnated sample was well mixed and then evaporated in a rotary evaporator at constant temperature of 353 K. The as-prepared sample was carefully washed with distilled water, dried at 353 K overnight, and then reduced in 5% H_2/95% He at 523 K for 1 h prior to being used as catalyst.

Characterization Techniques. The specific surface areas of samples were determined through N_2 adsorption/desorption isotherms at 77 K collected on a Quantachrome iQ-MP gas adsorption analyzer. The X-ray diffraction (XRD) patterns of TiO_2 samples were recorded on a Bruker D8 ADVANCE powder diffractometer using Cu Kα radiation (λ = 0.1542 nm) at a scanning rate of 4°/min in the region of 2θ = 10–80°. Transmission electron microscopy (TEM) images were taken on a FEI Tecnai G2 F30 microscope at an acceleration voltage of 200 kV. A few drops of an alcohol suspension containing the sample were placed on a carbon-coated copper grid, followed by evaporation at ambient temperature. The particle size distribution was obtained from TEM images, and the average particle size was calculated from $d = \sum n_i d_i^3 / \sum n_i d_i^2$. The dispersion of supported metals was determined by H_2 pulse adsorption on a chemisorption analyzer (Chemisorb 2720, Micromeritics). In a typical experiment, ca. 100 mg of sample in the quartz reactor was first reduced in 5% H_2/95% He at 523 K for 1 h and then treated in He at 523 K for 1 h to remove H_2 adsorbed on the surfaces of samples. After the temperature was lowered to 298 K in flowing He, pulses of H_2 were injected into the reactor every 1 min until there were no further changes in intensity of outlet H_2. The dispersion of the metal was calculated by assuming the equimolar adsorption of hydrogen on metal.

Catalytic Evaluation and Product Analysis. The hydrogenolysis of various substrates was performed in a high-pressure stainless autoclave (Xinyuan Chemical Machinery, Series CJK, 300 mL) at a stirring rate of 750 rpm. In a typical experiment, 0.2 g of catalyst, 1 g of substrate, and 100 mL of solvent (typically *n*-heptane) were well mixed in the autoclave and purged with pure N_2 at room temperature. The autoclave was rapidly heated to the desired temperature (413–493 K), and H_2 was introduced at different pressures (0–3 MPa) to initiate the reaction.

After the reaction, the liquid organic products were analyzed by gas chromatography (Shimadzu GC-2010) and gas chromatography–mass spectrometry (Shimadzu GCMS-QP2010 SE), both with a RXI-5MS column (30 m, 0.25 mm

DOI: 10.1021/acscatal.5b02180
ACS Catal. 2015, 5, 7199–7207

Table 1. Hydrogenolysis of 1-Hexadecanol over Different Catalysts[a]

catalyst	metal loading (wt %)	temp (K)	product selectivity (%)		reaction rate (mol/(h mol_{Me}))	TOR[b]
			n-pentadecane	*n*-hexadecane		
TiO_2	0	473			0	
Pt/TiO_2	1.61	473	10.4	89.6	17.19	57.3
Ir/TiO_2	1.59	473	11.4	88.6	81.33	212.1
Pd/TiO_2	1.64	473	55.4	44.6	2.73	7.6
Rh/TiO_2	1.95	453	81.1	18.9	34.31	76.2
Ru/TiO_2	1.62	473	89.6	10.4	49.65	171.2
Fe/TiO_2	9.85	493	45.5	54.5	0.15	
Co/TiO_2	9.62	493	78.9	21.1	0.51	
Ni/TiO_2	9.76	493	88.0	12.0	2.03	
Rh/CeO_2	1.79	473	>99.9	<0.01	18.69	66.7
Ru/SiO_2	1.64	473	96.8	3.2	12.21	58.1
Ru/ZrO_2	1.63	473	90.1	9.9	13.17	48.8
Ru/CeO_2	1.58	473	97.2	2.8	56.49	156.9
Ru/TiO_2	0.48	473	83.6	16.4	65.28	94.3
Ru/TiO_2	0.96	473	87.2	12.8	58.42	129.8
Ru/TiO_2	3.18	473	93.1	6.9	36.48	202.6

[a]Reaction conditions: 1.0 g of 1-hexadecanol, 100 mL of *n*-heptane, 0.2 g of catalyst, 3 MPa of H_2. [b]Turnover rate defined as moles of substrate converted per hour per exposed metal site.

i.d., stationary phase thickness 0.25 μm). Eicosane or dodecane was used as an internal standard for quantification. The following temperature program was employed: isothermal heating at 323 K for 5 min, heating to 573 K with a rate of 10 K/min, and isothermal heating at 573 K for 10 min. The gas products were qualitatively analyzed with a mass spectrometer (Pfeiffer Omnistar GSD 320). For all experiments, carbon balances of over 95% could be obtained according to the calculations through an internal standard method.

Calculation Methods and Models. The activation barriers, total energy changes with and without preadsorbed atomic oxygen, and the corresponding analyses were performed by self-consistent periodical density functional theory (DFT) calculations using the Vienna ab initio simulation package (VASP).[26,27] The electronic structures were calculated using DFT within the GGA-PW91 functional.[28] The projector augmented wave (PAW) scheme[29,30] was used to describe the inner cores, and the electronic states were expended in a plane wave basis with a kinetic cutoff energy of 400 eV. The transition states (TS) were located by three steps: the general NEB method[31,32] was employed to find an approximated TS, then the quasi-Newton algorithm was used to optimize the likely TSs until the force acting on the atom was smaller than 0.03 eV/Å, and finally the frequency analysis was carried out to confirm the TS. Typically, Ru (0001) is modeled by the p (5 × 4) unit cell of three layers that are separated by ~15 Å under vacuum. The optimized lattice constant is 2.75 Å. Since a relatively large unit cell was used in this study, only one Γ point was used to sample the first Brillouin zone.[33] The adsorption energy (E_{ads}) and the activation energy (E_a) were calculated by the following two formulas: $E_{ads} = E_{A/M} - E_M - E_A$ and $E_a = E_{TS} - E_{IS}$, respectively. Here $E_{A/M}$, E_M, E_A, E_{TS}, and E_{IS} indicate the calculated energies of the adsorbate, substrate, adsorption system, TS, and initial states, respectively.

RESULTS AND DISCUSSION

The physicochemical properties of catalyst supports employed and selected catalyst samples were characterized by several techniques, e.g. N_2 adsorption/desorption, ICP, XRD, and TEM. The support structures have been determined by XRD (Figure S1 in the Supporting Information), and the surface areas of supports are measured to be >50 m^2/g through N_2 adsorption/desorption analysis. All of the catalyst samples show the typical morphology of supported systems. For Ru/TiO_2, ruthenium particles of 2−5 nm are observed to evenly disperse on the TiO_2 support and the ruthenium particle size increases distinctly with increasing loading (Figure 1a−c). Typically, the average ruthenium size in 1.62% Ru/TiO_2 is observed to be 3.4 nm (Figure 1d−f), meaning that one ruthenium particle contains over 1000 ruthenium atoms. In this context, it is rational to propose that the Ru (0001) surface dominates in Ru/TiO_2 catalyst.

Palmitic acid is the most common fatty acid found in animals, plants, and microorganisms, and 1-hexadecanol is known as the important reaction intermediate from palmitic acid conversion. Therefore, 1-hexadecanol was selected as a model compound and the catalytic performance of supported metals was tested in the hydrogenolysis of 1-hexadecanol. As shown in Table 1, the catalytic activity and product selectivity are determined by the catalysts employed. Reaction products from the hydrogenolysis of carbon−oxygen bonds and adjacent carbon−carbon bonds, i.e. *n*-hexadecane and *n*-pentadecane (CH_4 as exclusive gaseous C-containing product), could be detected with TiO_2-supported metals as catalysts. The time-on-stream behaviors of the 1-hexadecanol hydrogenolysis (Figure S2 in the Supporting Information) show that the product selectivity does not change obviously with the progress of reaction in most cases, indicating the parallel hydrogenolysis of carbon−oxygen and carbon−carbon bonds. In very few cases, e.g. with Pd/TiO_2 as catalyst, changes in the product selectivity with the progress of the reaction could be observed, which should be due to the reconstruction of active sites during the reaction. Pt/TiO_2 and Ir/TiO_2 appear to be adequate catalysts for the hydrogenolysis of carbon−oxygen bonds, while Rh/TiO_2 and Ru/TiO_2 can be used for the hydrogenolysis of carbon−carbon bonds. This is the first report of the selective scission of carbon−carbon bonds in 1-hexadecanol with Rh/TiO_2 and Ru/TiO_2 as catalysts under relatively mild conditions. We also find that the support materials can influence the activity and product selectivity to a great extent. Remarkably, Rh/CeO_2 catalyst exhibits a perfect

DOI: 10.1021/acscatal.5b02180
ACS Catal. 2015, 5, 7199−7207

selectivity to *n*-pentadecane of >99.9% with a sustainable reaction rate of 18.69 mol/(h mol_{Rh}), revealing its potential application in organic synthesis. The metal loadings also influence the catalytic performance. For Ru/TiO_2, increasing the Ru loading from 0.48 to 3.18% leads to a gradual increase in *n*-pentadecane selectivity from 83.6 to 93.1% as well as a decrease in reaction rate from 65.28 to 36.48 mol/(h mol_{Ru}). The effects of catalyst supports and metal loadings on the catalytic performance are ascribed to changes in the metal sites: e.g., the exposed facets. To reveal the intrinsic activity of Ru/TiO_2 catalysts in 1-hexadecanol hydrogenolysis, the turnover rates, defined as moles of 1-hexadecanol converted per hour per exposed ruthenium site, were calculated at different ruthenium loadings. It is observed that the turnover rate increases from 94.3 to 202.6 h^{-1} with increasing ruthenium particle size: i.e., an increase in ruthenium loading from 0.48 to 3.18% (Table 1). In this context, a two-dimensional flat Ru (0001) surface should be the preferred active site in the reaction, which is very important for the modeling of ruthenium catalysts in theoretical calculations.

Ru/TiO_2 with a Ru loading of 1.62% was selected as a model catalyst for further investigations, and the same batches of catalysts exhibit perfect reproducibility in the hydrogenolysis reaction. The effects of reaction parameters on the hydrogenolysis of 1-hexadecanol over Ru/TiO_2 are summarized in Table 2 (reaction kinetics are shown in Figure S3 in the Supporting Information). An increase in the reaction temperature leads to a sharp increase in the reaction rate of the 1-hexadecanol hydrogenolysis as expected, while the product selectivity is quite similar. Arrhenius plots of the 1-hexadecanol hydrogenolysis over Ru/TiO_2 give quite similar apparent activation energies of 97.0 and 101.3 kJ/mol for the hydrogenolysis of carbon−oxygen and adjacent carbon−carbon bonds (Figure 2), respectively.

Table 2. Effects of Reaction Parameters on the Hydrogenolysis of 1-Hexadecanol[a]

temp (K)	H_2 pressure (MPa)	product selectivity (%)		reaction rate (mol/(h mol_{Me}))
		n-pentadecane	*n*-hexadecane	
413	3.0	88.2	11.8	1.23
433	3.0	88.9	11.1	4.74
453	3.0	89.2	10.8	17.71
473	3.0	89.6	10.4	49.65
473	2.0	90.2	9.8	48.81
473	1.0	90.7	9.3	47.94
473	0.5	92.3	7.7	47.46
473	0.1	93.7	7.3	5.28[b]
473	0			0

[a]Reaction conditions: 1.0 g of 1-hexadecanol, 100 mL of *n*-heptane, 0.2 g (1.62 wt % Ru) of Ru/TiO_2 catalyst. [b]Reaction stops after time on stream of 0.5 h.

The hydrogen pressure in the reaction system shows distinct effects on the hydrogenolysis performance of Ru/TiO_2. No reaction occurs in the absence of hydrogen, and atmospheric hydrogen, i.e. 0.1 MPa, could induce the hydrogenolysis reaction. The hydrogenolysis rate dramatically increases with increasing the hydrogen pressure to 0.5 MPa, while further increases in the hydrogen pressure only result in marginal increases. These observations hint at the fact of hydrogen-assisted dissociation of carbon−carbon bonds. It should be mentioned that carbon−carbon bond oxidative cleavage has been acknowledged as a side reaction accompanied by the oxidation of unbranched primary alcohols to the corresponding carboxylic acids.[34,35] We therefore propose a similarity in carbon−carbon bond dissociation between the α-carbon and β-carbon atoms of 1-hexadecanol assisted by hydrogen or oxygen. Theoretically, other reactants might also assist the dissociation of carbon−carbon bonds, which is of great significance to the design of a synthetic methodology.

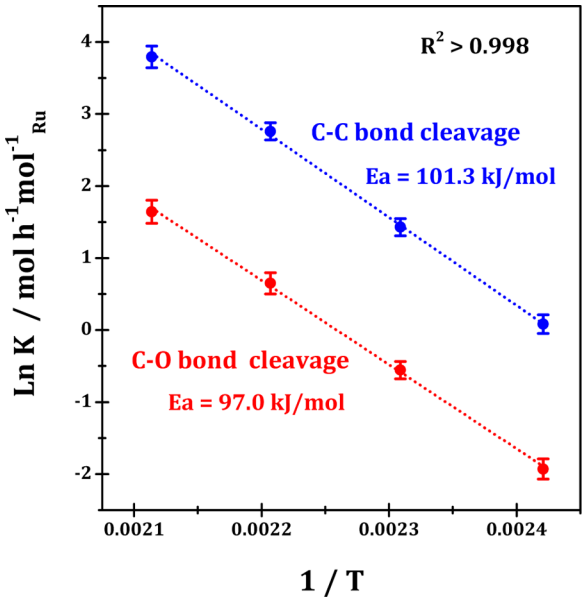

Figure 2. Arrhenius plots of the 1-hexadecanol hydrogenolysis catalyzed by Ru/TiO_2.

The hydrogenolysis of a series of primary aliphatic alcohols over Ru/TiO_2 has been investigated. As shown in Table 3 (reaction kinetics are shown in Figure S4 in the Supporting Information), preferential hydrogenolysis of carbon−carbon bonds over carbon−oxygen bonds (ca. 90% versus ca. 10%) can be obtained in all cases, demonstrating the universal feature of

Table 3. Hydrogenolysis of Primary Aliphatic Alcohols over Ru/TiO_2[a]

substrate	product distribution[b]		reaction rate (mol/(h mol_{Me}))
1-hexanol	90.5% *n*-pentane	9.5% *n*-hexane	128.19
1-decanol	89.7% *n*-nonane	10.3% *n*-decane	62.46
1-dodecanol	89.5% *n*-hendecane	10.5% *n*-dodecane	55.56
1-tetradecanol	91.7% *n*-tridecane	8.3% *n*-tetradecane	52.14
1-hexadecanol	89.6% *n*-pentadecane	10.4% *n*-hexadecane	49.65
1-octadecanol	90.0% *n*-heptadecane	10.0% *n*-octadecane	43.18
1-eicosanol	91.1% *n*-nonadecane	8.9% *n*-eicosane	37.47
1-docosanol	89.3% *n*-heneicosane	10.7% *n*-docosane	33.09

[a]Reaction conditions: 1.0 g of substrate, 100 mL of *n*-heptane, 0.2 g (1.62 wt % Ru) of Ru/TiO_2 catalyst, 3 MPa of H_2, 473 K. [b]At time on stream of 6 h.

DOI: 10.1021/acscatal.5b02180
ACS Catal. 2015, 5, 7199−7207

such types of reactions. In addition, a noticeable increase in the reaction rate could be obtained with decreasing carbon number in primary alcohol. We further investigated the hydrogenolysis of different substrates over Ru/TiO_2 for a better understanding of these types of reactions, and the results are summarized in Table 4 (reaction kinetics are shown in Figure S5 in the Supporting Information). When 1-chlorohexadecane or 1-bromohexadecane was employed as substrate, only the hydrogenolysis of carbon−halogen bond took place and *n*-hexadecane was observed as the exclusive product. The hydrogenolysis of 1-hexadecanethiol and 1-hexadecanamine at 473 K was rather slow and, therefore, we increased the reaction temperature to 493 K to obtain discernible kinetic data. Hydrogenolysis of 1-hexadecanethiol gave *n*-hexadecane and its isomer as the dominant products together with a considerable amount of *n*-hexadecene. This implies the exclusive hydrogenolysis of carbon−sulfur bonds instead of carbon−carbon bonds, with H_2S detected as the exclusive gaseous product (Figure S6 in the Supporting Information). The reaction process should be H_2S elimination followed by hydrogenation. However, due to the poisoning of Ru/TiO_2 by H_2S, some *n*-hexadecane could not be hydrogenated and, therefore, detected as product. Hydrogenolysis of 1-hexadecanamine gave both *n*-hexadecene (38.3%) and *n*-pentadecane (40.2%), indicating the simultaneous cleavage of carbon−carbon and carbon−nitrogen bonds (NH_3 detected as gaseous product, Figure S6). However, the high reaction temperature would probably lead to the successive hydrogenolysis of alkane products and some alkanes with lower carbon numbers could be detected (CH_4 as exclusive C-containing gaseous product; Figure S6). In addition to the type of functional group, the position of the functional group, i.e. hydroxyl, in *n*-hexadecane has a distinct effect on the hydrogenolysis process. The hydrogenolysis of secondary alcohols generally gives *n*-hexadecane as the dominant product. Typically, the hydrogenolysis of 8-hexadecanol produces exclusively *n*-hexadecane, while the hydrogenolysis of 2-hexadecanol produces 69.1% *n*-hexadecane together with 5.9% *n*-pentadecane and 18.6% *n*-tetradecane. The different behaviors should be due to the small difference in the carbon−carbon bond energies at different positions and the resulting different reaction pathways. For the hydrogenolysis of cyclohexanol, a type of secondary alcohol, cyclohexane, was obtained as the exclusive product. In contrast, the hydrogenolysis of primary alcohols with a substituted cyclohexyl group, e.g. cyclohexylmethanol and cyclohexylethanol, underwent the preferential cleavage of carbon−carbon bonds over carbon−oxygen bonds.

Table 4. Hydrogenolysis of Different Substrates over Ru/TiO_2[a]

substrate	product distribution[b]	reaction rate (mol/(h mol_{Me}))
1-hexadecanol	10.4% *n*-hexadecane	49.65
	89.6% *n*-pentadecane	
1-hexadecanethiol[c]	55.2% *n*-hexadecane	5.91
	27.2% hexadecane isomer	
	17.6% n-hexadecene	
1-hexadecanamine[c]	38.3% *n*-hexadecane	11.04
	40.2% *n*-pentadecane	
	11.2% *n*-tetradecane	
	6.0% *n*-tridecane	
	2.2% *n*-fodecane	
	1.6% *n*-hendecane	
2-hexadecanol	69.1% *n*-hexadecane	13.22
	5.9% *n*-pentadecane	
	18.6% *n*-tetradecane	
	1.8% *n*-tridecane	
	1.7% *n*-fodecane	
8-hexadecanol	>99.9% *n*-hexadecane	26.37
1-chlorohexadecane	>99.9% *n*-hexadecane	7.63
1-bromohexadecane	>99.9% *n*-hexadecane	4.78
cyclohexanol[d]	>99.9% cyclohexane	13.56
cyclohexylmethanol[d]	90.7% cyclohexane	128.19
	9.3% methylcyclohexane	
cyclohexylethanol[d]	90.6% methylcyclohexane	109.26
	9.4% ethylcyclohexane	

[a]Reaction conditions: 1.0 g of substrate, 100 mL of *n*-heptane, 0.2 g (1.62 wt % Ru) of Ru/TiO_2 catalyst, 3 MPa of H_2, 473 K, unless specifically stated. [b]At time on stream of 6 h; only fractions greater than 1.5% are shown. [c]Reaction temperature of 493 K. [d]100 mL of isooctane used as solvent instead of *n*-heptane.

Reaction Mechanism for the 1-Hexadecanol Hydrogenolysis. On the basis of the catalytic results presented, the hydrogenolysis of 1-hexadecanol undergoes distinctly different reaction mechanisms with different catalysts. For Ru catalysts, two parallel pathways, i.e. carbon−carbon bond scission and carbon−oxygen bond scission, run simultaneously during the 1-hexadecanol hydrogenolysis.

Hereafter, Ru metals are selected as model catalysts for the 1-hexadecanol hydrogenolysis for an insight of the selective bond fission. The adsorption properties of important intermediate species involved in the 1-hexadecanol hydrogenolysis processes are given in Table S1 in the Supporting Information, with which the associated reaction mechanism could be investigated in detail. The calculated reaction energies, energy barriers, and bond lengths of transition states (TS) on a flat Ru (0001) surface are shown in Table 5, and the optimized TS configurations of some key steps are shown in Figure 3.

Generally, the whole reaction network can be divided into three parts: (i) C−O versus C−C bond scission, (ii) hydrogenation of the resulting species, and (iii) CO hydrogenation into methane.

(i). C−O versus C−C Bond Scission. The initial possible bond scission of 1-hexadecanol on flat Ru (0001) includes α-carbon−hydrogen, β-carbon−hydrogen, oxygen−hydrogen, carbon−carbon,and carbon−oxygen bond cleavage, and the reaction should start with the breaking of an oxygen−hydrogen bond, with the smallest energy barrier of 0.79 eV and the longest bond length of 1.99 Å, to generate $C_{14}H_{29}CH_2CH_2O$ species. The breaking of α-carbon−hydrogen and β-carbon−hydrogen bonds are two possible paths for the dehydrogenation of $C_{14}H_{29}CH_2CH_2O$ species, while the breaking of the former (0.73 eV) is energetically favored over that of the latter (1.00 eV). The generated $C_{14}H_{29}CH_2CHO$ species prefer to go on to the breaking of an α-carbon−hydrogen bond (0.28 eV) over that of β-carbon−hydrogen bond (0.50 eV), followed by abstraction of (β-carbon-)hydrogen (0.54 eV) to generate $C_{14}H_{29}CHCO$ species.

The $C_{14}H_{29}CHCO$ species may undergo the breaking of a carbon−oxygen (1.21 eV) or carbon−carbon bond (1.11 eV), leading to the formation of $C_{14}H_{29}CHC$ or $C_{14}H_{29}CH$ species, respectively. Both of these steps are exothermic, and the

DOI: 10.1021/acscatal.5b02180
ACS Catal. 2015, 5, 7199−7207

Table 5. Calculated Reaction Energies (ΔH), Energy Barriers (E_a), and Bond Lengths of TS on a Ru (0001) Flat Surface

reaction step	ΔH (eV)	E_a (eV)	d (Å)
$RCH_2CH_2OH + * \rightarrow RCH_2CH_2OH*$	−0.42		
$RCH_2CH_2OH* \rightarrow RCH_2CHOH* + H*$	0.13	0.86	1.60
$RCH_2CH_2OH* \rightarrow RCH_2CH_2O* + H*$	−0.57	0.79	1.41
$RCH_2CH_2OH* \rightarrow RCHCH_2OH* + H*$	0.21	1.08	1.73
$RCH_2CH_2O* \rightarrow RCH_2CHO* + H*$	0.02	0.73	1.56
$RCH_2CH_2O* \rightarrow RCHCH_2O + H*$	0.27	1.00	1.65
$RCH_2CHO* \rightarrow RCH_2CO* + H*$	−0.30	0.28	1.20
$RCH_2CHO* \rightarrow RCHCHO* + H*$	−0.43	0.50	1.64
$RCH_2CO \rightarrow RCHCO + H*$	−0.10	0.54	1.57
$RCHCO* \rightarrow RCHC* + O*$	−0.36	1.21	1.87
$RCHCO* \rightarrow RCH* + CO*$	−0.41	1.11	2.02
$RCH* + H* \rightarrow RCH_2*$	0.39	0.71	1.69
$RCH_2* + H* \rightarrow RCH_3$	−0.18	0.68	1.72
$RCHC* + H* \rightarrow RCHCH*$	0.01	0.27	1.66
$RCHCH* + H* \rightarrow RCH_2CH*$	0.22	0.51	1.65
$RCH_2CH* + H* \rightarrow RCH_2CH_2*$	0.39	0.71	1.69
$RCH_2CH_2* + H* \rightarrow RCH_2CH_3$	−0.18	0.68	1.72
$CO* \rightarrow C* + O*$	0.42	>2	
$CO* \rightarrow CO + *$	1.98		
$CO* + H* \rightarrow HCO*$	24.4	1.21	1.14
$HCO* + H* \rightarrow H_2CO*$	0.39	0.31	1.52
$H_2CO* \rightarrow CH_2* + O*$	−0.68	0.78	2.01
$CH_2* + H* \rightarrow CH_3*$	0.06	0.55	1.64
$CH_3* + H* \rightarrow CH_4$	−0.18	0.67	1.57

barriers are low enough for reaction under conditions employed in this study. The carbon−carbon bond scission in $C_{14}H_{29}CHCO$ species appears to be the preferred step, due to its smaller energy barrier in comparison with that of carbon−oxygen bond scission.

(ii). Hydrogenation of the Resulting Species. The $C_{14}H_{29}CH$ species undergo two successive hydrogenation steps to generate the final product $C_{14}H_{29}CH_3$. The first hydrogenation is endothermic, while the second hydrogenation is exothermic. However, both hydrogenation steps carry a similarly small barrier of ∼0.7 eV.

$C_{14}H_{29}CHC$ species need four steps for hydrogenation to generate the final product $C_{14}H_{29}CH_2CH_3$. The hydrogenation may take place on an α-carbon or β-carbon, and the most feasible hydrogenation pathway is established as $C_{14}H_{29}CHC \rightarrow C_{14}H_{29}CHCH \rightarrow C_{14}H_{29}CH_2CH \rightarrow C_{14}H_{29}CH_2CH_2 \rightarrow C_{14}H_{29}CH_2CH_3$. All of the hydrogenation steps carry small barriers of below 0.8 eV, indicating that the hydrogenation is facile.

(iii). CO Hydrogenation into Methane. When CO is formed on the surface from carbon−carbon bond scission, it should desorb or react further. Since the CO desorption energy (1.98 eV) or CO dissociation energy (>2 eV) is much larger than the barrier for hydrogenation (1.21 eV) on Ru (0001), the adsorbed CO prefers to undergo further hydrogenation processes. The detailed pathway for CO hydrogenation is established as $CO* \rightarrow HCO* \rightarrow H_2CO* \rightarrow CH_2* \rightarrow CH_3* \rightarrow CH_4$. The first hydrogenation ($CO* + H* \rightarrow HCO* + *$) is denoted as the rate-controlling step with the largest reaction barrier, similar to previous reports on Rh (111).[36] Once CH_4 is formed, it does not stick to the Ru (0001) surface and desorbs as a gaseous product, in line with experimental observations of methane as the exclusive gaseous product (Figure S6 in the Supporting Information). The overall reaction $CO* + 6H* \rightarrow CH_4 + H_2O$ is highly exothermic, indicating that the formation of CH_4 is thermodynamically favorable.

It is interesting to note that the hydrogenation of adsorbed CO to formyl species is also the rate-controlling step for the 1-hexadecanol hydrogenolysis to *n*-pentadecane, due to its greater barrier over other elementary steps. The hydrogenation of adsorbed CO species on Ru (0001) is not involved in the elementary reaction steps for the 1-hexadecanol hydrogenolysis to *n*-hexadecane; however, it has a huge effect on *n*-hexadecane production, considering that sufficient free sites on Ru (0001) surface are required for the reaction. That is, the active sites for *n*-hexadecane production during the reaction are poisoned by the strongly adsorbed CO species from its parallel reaction, *n*-pentadecane production. In this context, adequate external energy is required during the 1-hexadecanol hydrogenolysis to overcome the energy barrier for the removal of adsorbed CO and the recovery of a clean Ru (0001) surface.

The complete energy profile of the 1-hexadecanol hydrogenolysis on flat Ru (0001) is shown in Figure 4. The intrinsic overall barriers are observed to be, as it happens, 1.21 eV both for the production of *n*-hexadecane and for the production of *n*-pentadecane, in line with the similar experimental apparent barriers of 101.3 and 97.0 kJ/mol, respectively (Figure 2). The removal of adsorbed CO ($CO* + 6H* \rightarrow CH_4 + H_2O$) on the Ru (0001) surface is acknowledged as a crucial step for the 1-hexadecanol hydrogenolysis. On the one hand, it contributes to the largest energy barrier of 1.21 eV and is the rate-controlling step for *n*-pentadecane production. On the other hand, it also retards the rate for *n*-hexadecane production due to the covering of Ru (0001) sites by strongly adsorbed CO species. As a result, the 1-hexadecanol hydrogenolysis on Ru (0001) undergoes two parallel pathways, and *n*-pentadecane and *n*-hexadecane are produced simultaneously. Considering that the carbon−carbon bond scission carries an energy barrier smaller than carbon−oxygen bond scission, *n*-pentadecane is observed as the dominant product from the 1-hexadecanol hydrogenolysis on Ru (0001). On the basis of the theoretical calculations, it can be expected that C−O versus C−C bond scissions are key factors determining the product distribution from aliphatic alcohol hydrogenolysis. We further calculated the energy barriers for these two steps on other possible exposed surfaces: i.e., stepped Ru (0001) and Ru (100) (optimized IS and TS configurations are shown in Figures S7 and S8 in the Supporting Information). The results are summarized in Table 6. It is clearly seen that C−O bond scission is preferred on stepped Ru (0001) and Ru (100), while C−C bond scission is preferred on flat Ru (0001). Since flat Ru (0001) constitutes the dominating exposed facets in 1.62% Ru/TiO_2, the selective scission of C−C bonds is observed in 1-hexadecanol hydrogenolysis. Regardless, it can be stated that the selective catalytic bond fission during aliphatic alcohol hydrogenolysis is not only controlled by the types of active metals but also controlled by their exposed facets.

These results can explain the effects of supports and metal loadings on the catalytic behaviors of ruthenium catalysts well (Table 1) and can also provide a potential strategy to adjust the product distribution from aliphatic alcohol hydrogenolysis. Preliminary results indicate that the introduction of 0.5% potassium or calcium to Ru/TiO_2 can increase the *n*-pentadecane selectivity, while the introduction of 0.5% vanadium can significantly increase the *n*-pentadecane

DOI: 10.1021/acscatal.5b02180
ACS Catal. 2015, 5, 7199−7207

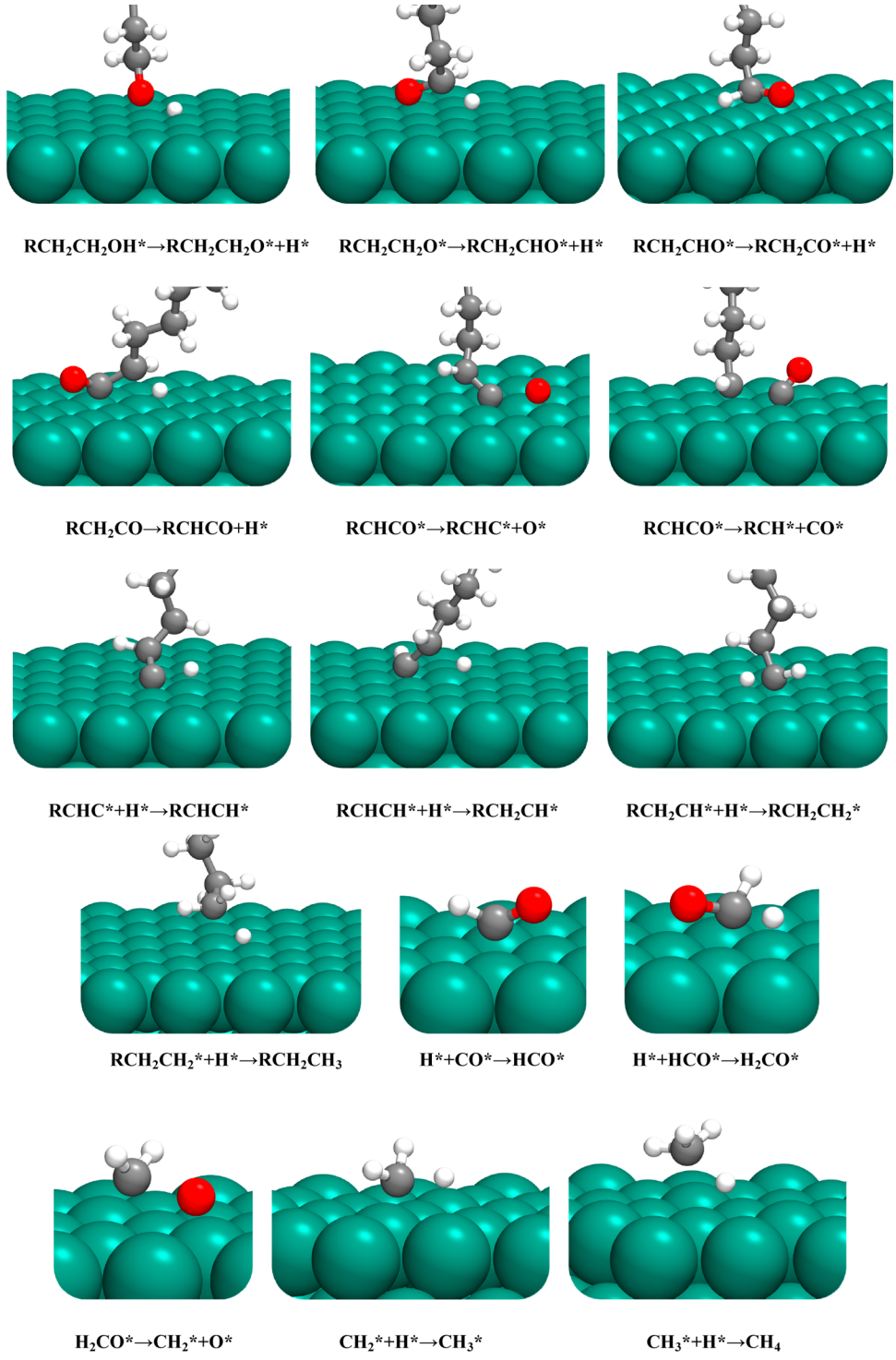

Figure 3. Optimized TS configurations of key steps on flat Ru (0001).

selectivity during 1-hexadecanol hydrogenolysis (Figure S9 in the Supporting Information).

CONCLUSION

In contrast to the conventional thinking that the cleavage of carbon−carbon σ bonds is difficult due to their high binding energies, the selective hydrogenolysis of carbon−carbon σ bonds in primary aliphatic alcohols is achieved with supported metals as heterogeneous catalysts under relatively mild conditions. For 1-hexadecanol hydrogenolysis, the catalyst-controlled selective scission of carbon−oxygen bonds or adjacent carbon−carbon bonds is clearly illustrated. With Ru/TiO_2 as a model catalyst, the scission of carbon−carbon bonds is preferred over carbon−oxygen bonds, resulting in *n*-pentadecane as the dominant product with a small quantity of *n*-hexadecane. Theoretical calculations reveal that 1-hexadecanol hydrogenolysis on flat Ru (0001) simultaneously undergoes carbon−carbon bond scission to produce *n*-pentadecane and carbon−oxygen bond scission to produce *n*-hexadecane. The removal of adsorbed CO on a flat Ru (0001)

DOI: 10.1021/acscatal.5b02180
ACS Catal. 2015, 5, 7199−7207

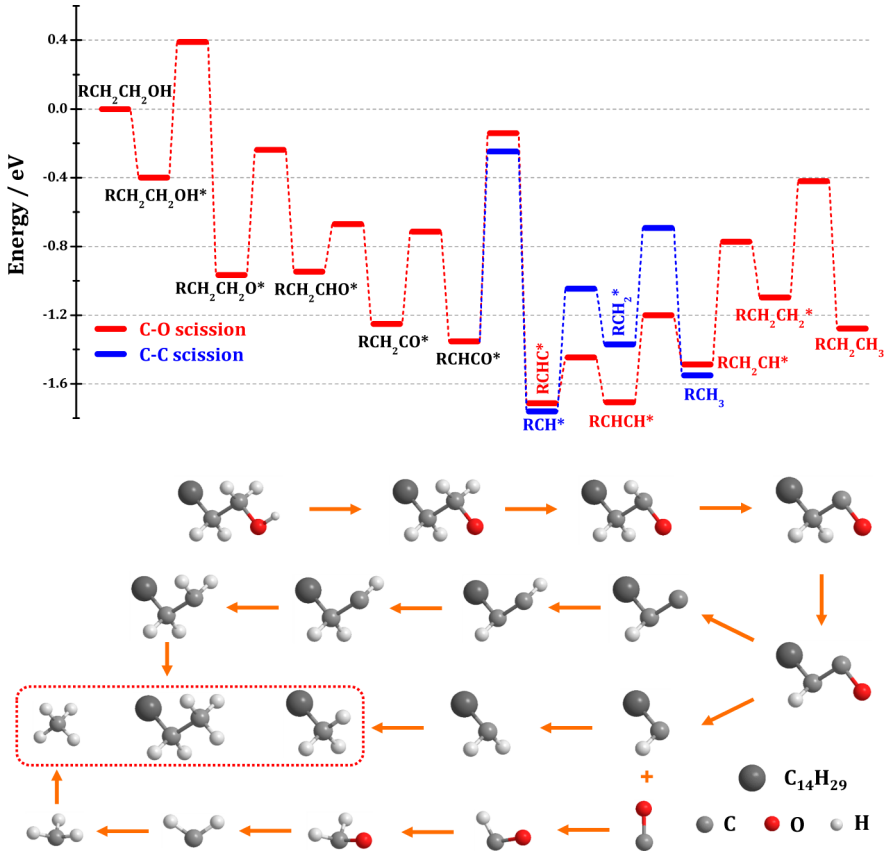

Figure 4. Calculated energy profile and reaction pathway for the 1-hexadecanol hydrogenolysis to *n*-hexadecane and *n*-pentadecane on flat Ru (0001).

Table 6. C−O Bond versus C−C Bond Scission on Different Ruthenium Surfaces

	reaction step (eV)		
surface	RCHCO* → RCH* + CO*	RCHCO* → RCHC* + O*	CO* + H* → HCO* + *
flat Ru (0001)	1.11	1.21	1.21
stepped Ru (0001)	1.06	0.44	
Ru (100)	1.17	0.96	

surface contributes to the largest energy barrier in *n*-pentadecane production, and it also retards the rate for *n*-hexadecane production by covering the active Ru (0001) surface. These results improve our fundamental understanding of catalyst-controlled carbon−carbon σ bond scission and also shed light on the design of selective catalysts for organic transformations.

■ ASSOCIATED CONTENT

Supporting Information

The Supporting Information is available free of charge on the ACS Publications website at DOI: 10.1021/acscatal.5b02180.

Adsorption energies and configurations of key reaction intermediates, optimized initial and transition state configurations of key steps, XRD patterns of catalyst supports, time on stream behaviors of hydrogenolysis reactions, and mass spectrometry analysis of gaseous products (PDF)

■ AUTHOR INFORMATION

Corresponding Author

*L.L.: e-mail, lild@nankai.edu.cn; fax, +86-22-2350-0341.

Author Contributions

‖These authors contributed equally to this work.

Notes

The authors declare no competing financial interest.

■ ACKNOWLEDGMENTS

This work was supported by the National Natural Science Foundation of China (21373119, 21421001), the Ministry of Education of China (IRT13022), and the 111 project (B12015).

■ REFERENCES

(1) Jun, C. H.; Lee, H. *J. Am. Chem. Soc.* **1999**, *121*, 880−881.
(2) Park, Y. J.; Park, J. W.; Jun, C. H. *Acc. Chem. Res.* **2008**, *41*, 222−234.
(3) Szajna, E.; Arif, A. M.; Berreau, L. M. *J. Am. Chem. Soc.* **2005**, *127*, 17186−17187.
(4) Allpress, C. J.; Grubel, K.; Szajna-Fuller, E.; Arif, A. M.; Berreau, L. M. *J. Am. Chem. Soc.* **2013**, *135*, 659−668.
(5) Allpress, C. J.; Berreau, L. M. *Coord. Chem. Rev.* **2013**, *257*, 3005−3029.
(6) Sergeev, A. G.; Hartwig, J. F. *Science* **2011**, *332*, 439−443.
(7) Atesin, A. C.; Ray, N. A.; Stair, P. C.; Marks, T. J. *J. Am. Chem. Soc.* **2012**, *134*, 14682−14685.
(8) Wilsily, A.; Nguyen, Y.; Fillion, E. *J. Am. Chem. Soc.* **2009**, *131*, 15606−15607.
(9) Chen, K.; Li, H.; Lei, Z. Q.; Li, Y.; Ye, W. H.; Zhang, L.-S.; Sun, J.; Shi, Z. J. *Angew. Chem., Int. Ed.* **2012**, *51*, 9851−9855.

DOI: 10.1021/acscatal.5b02180
ACS Catal. 2015, 5, 7199−7207

(10) Maier, W. F.; Grubmüller, P.; Thies, I.; Stein, P. M.; McKervey, M. A.; Schleyer, P. v. R. *Angew. Chem., Int. Ed. Engl.* **1979**, *18*, 939−940.
(11) Grubmüller, P.; Schleyer, P. v. R.; McKervey, M. A. *Tetrahedron Lett.* **1979**, *20*, 181−184.
(12) Kochloefl, K.; Bažant, V. *J. Catal.* **1967**, *8*, 250−260.
(13) Kochloefl, K.; Bažant, V. *J. Catal.* **1968**, *10*, 140−148.
(14) Leclercq, G.; Leclercq, L.; Maurel, R. *J. Catal.* **1976**, *44*, 68−75.
(15) Leclercq, G.; Leclercq, L.; Maurel, R. *J. Catal.* **1977**, *50*, 87−97.
(16) Lecuyer, C.; Quignard, F.; Choplin, A.; Olivier, D.; Basset, J. M. *Angew. Chem., Int. Ed. Engl.* **1991**, *30*, 1660−1661.
(17) Corker, J.; Lefebvre, F.; Lecuyer, C.; Dufaud, V.; Quignard, F.; Choplin, A.; Evans, J.; Basset, J. M. *Science* **1996**, *271*, 966−969.
(18) Rosier, C.; Niccolai, G. P.; Basset, J. M. *J. Am. Chem. Soc.* **1997**, *119*, 12408−12409.
(19) Chabanas, M.; Vidal, V.; Coperet, C.; Thivolle-Cazat, J.; Basset, J. M. *Angew. Chem., Int. Ed.* **2000**, *39*, 1962−1965.
(20) Wojcik, B.; Adkins, H. *J. Am. Chem. Soc.* **1933**, *55*, 1293−1294.
(21) Peng, B.; Yuan, X.; Zhao, C.; Lercher, J. A. *J. Am. Chem. Soc.* **2012**, *134*, 9400−9405.
(22) Gosselink, R. W.; Stellwagen, D. R.; Bitter, J. H. *Angew. Chem., Int. Ed.* **2013**, *52*, 5089−5092.
(23) Zhao, C.; Brück, T.; Lercher, J. A. *Green Chem.* **2013**, *15*, 1720−1739.
(24) Rozmysłowicz, B.; Kirilin, A.; Aho, A.; Manyar, H.; Hardacre, C.; Wärnå, J.; Salmi, T.; Murzin, D. Y. *J. Catal.* **2015**, *328*, 197−207.
(25) Gürbüz, E. I.; Hibbitts, D. D.; Iglesia, E. *J. Am. Chem. Soc.* **2015**, *137*, 11984−11995.
(26) Kresse, G.; Furthmüller, J. *Comput. Mater. Sci.* **1996**, *6*, 15−50.
(27) Kresse, G.; Furthmüller, J. *Phys. Rev. B: Condens. Matter Mater. Phys.* **1996**, *54*, 11169−11181.
(28) Perdew, J. P.; Wang, Y. *Phys. Rev. B: Condens. Matter Mater. Phys.* **1992**, *45*, 13244−13249.
(29) Blöchl, P. E. *Phys. Rev. B: Condens. Matter Mater. Phys.* **1994**, *50*, 17953−17979.
(30) Kresse, G.; Joubert, D. *Phys. Rev. B: Condens. Matter Mater. Phys.* **1999**, *59*, 1758−1775.
(31) Mills, G.; Jonsson, H. *Phys. Rev. Lett.* **1994**, *72*, 1124−1127.
(32) Henkelman, G.; Uberuaga, B. P.; Jonsson, H. *J. Chem. Phys.* **2000**, *113*, 9901−9904.
(33) Monkhorst, H. J.; Pack, J. D. *Phys. Rev. B* **1976**, *13*, 5188−5192.
(34) Tojo, G.; Fernandez, M. *Oxidation of primary alcohols to carboxylic acids. A guide to current common practice*; Springer: Berlin, 2007.
(35) Bekish, A. V. *Tetrahedron Lett.* **2012**, *53*, 3082−3085.
(36) Choi, Y.; Liu, P. *J. Am. Chem. Soc.* **2009**, *131*, 13054−13061.

DOI: 10.1021/acscatal.5b02180
ACS Catal. 2015, 5, 7199−7207